Linear splay elasticity in surface-induced films of tilted smectic liquid crystals

Yves Galerne* and Rachid Najjar
Institut de Physique et Chimie des Matériaux de Strasbourg, 23 rue du Læss, BP 43, 67034 Strasbourg, France
(Received 13 October 2003; published 24 March 2004)

The prefrozen films that may be observed at the surface of isotropic liquid crystal droplets, close to the isotropic-smectic phase transition, or surface-induced films, are essentially asymmetric. If moreover, the molecules are tilted inside the smectic layers, as in the smectic-C (SmC) or smectic-C_A (SmC_A) phases, the **c** director that we may define as the order parameter of the film, is a real vector. Thus, the surface-induced films of MHTAC exhibit vectorial or polar properties, though the molecules are not chiral. The film free energy therefore contains a surface-elasticity term, $K_1\mathbf{c}^2\boldsymbol{\nabla}\cdot\mathbf{c}$, that is a linear function of the splay distortion, and that may be negative enough to promote a mechanical instability. A spontaneous **c** distortion, or **c** modulation, then invades the whole film and produces an array of parallel stripes, with a typical four-fringe periodicity when observed between crossed polarisers. Here, we present optical measurements of the distortion for different film thicknesses, and we propose a linear analysis of the data to test our model. Due to the limitations inherent to the Fourier expansion that we use, the calculations are valid only between two limits: a large q limit where splay domains collapse into disclination lines, and a small q borderline below which the distortion evolves towards a system of independent solitons. We find that the sign of the spontaneous splay elastic constant K_1 alternates as a function of the number of layers, N, a property that is reminiscent of the alternate structure of the SmC_A phase. We argue that the two-dimension elastic constant, K_1, originates from the interactions between the molecules in contact to the isotropic phase, and we deduce $K_1 \sim -(-1)^N \times 10^{-11}$ N and the elastic anisotropy, with a ratio of the splay over bend elastic constants $K_s/K_b \sim 4.5$. Similar properties could be observed also in other types of ultrathin films, e.g., in free-standing, ferroelectric (SmC^*) or antiferroelectric (SmC_A^*), films, in Langmuir films, and even in particular biological films. In some cases, a second, electric instability may occur and superimpose onto the elastic one.

DOI: 10.1103/PhysRevE.69.031706 PACS number(s): 61.30.Gd, 68.05.Cf, 68.15.+e, 64.70.Md

I. INTRODUCTION

Periodic morphologies are rather ubiquitous; they may be observed in a wide variety of systems belonging to both hard and soft matter physics. They may be observed in superconductors, in magnetic solids, in ferrofluids, and in organic systems as well, in two or three dimensions. From an experimental point of view, they are more easily evidenced in two-dimensional systems where imaging techniques may be used. They then yield textures that reveal to be sometimes beautiful, always surprising [1]. This probably explains in part that they have been intensively studied in the past years.

The morphologies have different physical origins. Except in the trivial case where the observed periodic texture directly results from some intrinsic period of the structure, they are produced by instabilities that are due to a competition between two antagonistic effects. However, this competition between antagonistic forces really exists only if the system exhibits enough fluidity to evolve towards its free energy minimum. Let us also note that the competition may develop in a static way, or dynamically, as for instance in the case of the Rayleigh-Bénard instability.

The resulting periodic textures may be rather complicated, with more or less regular arrays of domains, fingerprints, labyrinths, etc., sometimes exhibiting several characteristic lengths. In the simplest case, the periodic phenomena arise along one direction only, and they draw patterns of parallel and equidistant stripes, perpendicular to an **x** axis. Though produced by different physical mechanisms, the instabilities may keep the same appearance. In that sense, their mere observation is insufficient to lead to a unique interpretation. Nevertheless, provided characteristic features are correctly measured, they may be used as an indirect, but powerful, tool for studying the physical effects under competition, and to obtain interesting insights into the physics of the system.

Liquid crystals are well-suited to observe instabilities, because they are fluid and easy to prepare in two-dimensional (2D) films. Moreover, they exhibit many different phases [2]. Some of them are close to biological systems and may somehow mimic them. A simple method to make liquid crystal films consists of spreading them at the free surface of water, or of glycerin. Asymmetric films a few molecules thick, or Langmuir films, may be prepared in this way. Under particular conditions, they exhibit interesting patterns with domains [3–5], stripes or spirals [6–8]. Again, they are produced by different mechanisms. In the case of thin nematic films spread at the free surface of glycerin, the instability is shown to be promoted by surface-like elastic terms, K_{13} and K_{24} [7]. With smectic-C Langmuir monolayers at the free surface of water, a different mechanism that involves an interaction between two order parameters, is invoked to explain the mechanism of the instability [8].

Liquid crystals may also rather easily be conditioned in free-standing films held on a frame [9]. The film naturally exhibits the required fluidity mentioned above to allow instabilities to form. Again, the film may be processed in different phases, giving the opportunity to observe several types of

*Email address: Yves.Galerne@ipcms.u-strasbg.fr

instabilities. Stripes and multiarmed stars are thus observed in hexatic films of achiral liquid crystals [10]. Stripe textures are commonly observed in free-standing films of the ferroelectric smectic C^* (SmC^*) phase [11,12], together with possible square lattices [13,14]. They may similarly be observed in achiral freely suspended smectic C films [15].

Liquid crystals are a very versatile molecular system. They allow one to realize a third type of free thin film, somewhat intermediate between the Langmuir films and the free-standing films, in the sense that they are obtained with pure molecular systems. They are the prefreezing films that appear at the free surface of isotropic liquid crystal droplets, slightly above the isotropic phase transition, and that are indeed smectic films induced by the surface field [16]. They are analogous to the premelting films [17]. However, conversely to most materials, they constitute a remarkable exception since, as in the alcanes, they are in a more ordered phase than the bulk. In addition, the prefreezing films observed in liquid crystals, cannot grow more than a few molecular layers. If one tries to make them thicker, for instance by cooling the temperature, they become instable, and suddenly all the sample turns out to the smectic phase [18]. In that sense, they also may be considered as prewetting films. Interestingly also, being somehow half free-standing films, they are dissymmetric with two different interfaces. This property is essential concerning the physical effects we discuss here.

With no contact to solid substrates, except at their boundaries, all three types of films are mechanically free. They are therefore completely fluid and, not being submitted to anchoring effects, after a while, they reach to their equilibrium state. In this manner, these three mechanical systems are particularly convenient for experimental studies on subtle physical effects that are not usually observed. Moreover, they are two-dimensional systems that have different, and not very well-known properties, compared to the three-dimensional, bulk ones. Another interesting feature of these systems is that they are almost perfectly well oriented, with the smectic layers being parallel to the free surface. They appear to be driven by surface tension that is a very strong force at the molecular scale. This orientation property is important if one considers that a major experimental problem in liquid crystal research essentially concerns the orientation of the sample itself.

In this paper, we focus on smectic prefreezing films that are induced at the free surface of isotropic liquid crystal puddles [Fig. 1(a)] and more specifically, on the case where the molecules are achiral, and tilted by an angle θ inside the layers. We take advantage of the existence of mechanical instabilities to evidence a linear splay energy that has received little attention up to now [19–23]. We show that this energy has significant consequences on the physical properties of asymmetric films, a few smectic layers thick. In particular, it may give different widths to the splay distortions according to their signs, while correspondingly the smectic tilt angle is modulated. On using symmetry arguments, we deduce that the linear splay energy involved in the surface-induced films is a surface energy (Sec. II). We corroborate this point experimentally on performing measurements of

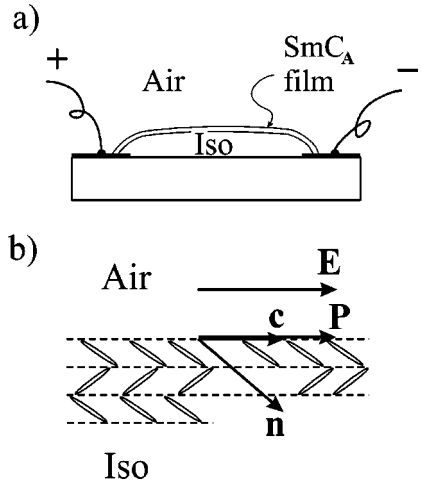

FIG. 1. Smectic C_A film induced at the free surface of an isotropic droplet of MHTAC liquid crystal. The film is observed in transmitted light between crossed polarizers. (a) General view. (b) Detailed sketch of a two-layer-thick film with an edge dislocation at the front of a new smectic layer. The horizontal component of the electric polarization **P** only, is represented.

distortions for different thicknesses of the film, obtained on slightly changing temperature (Sec. III). We thus verify that its relative importance increases when the film thickness is decreased. In particular, it may become large enough to distort the film spontaneously, giving it a lower free energy than in the uniform orientation. This may explain the mechanism of the instability observed in the form of arrays of distortion walls. To make it clearer, we propose a linear analysis of the distortion, based on its Fourier expansion up to the second harmonics (Sec. IV). This process yields a support to discuss our experimental results in more details (Sec. V). Though the experimental results that we present here are essentially obtained on surface-induced films with a particular compound, we may argue that in fact, the effect should be really ubiquitous and exist too in the Langmuir films and in the free-standing films, though in a slightly different form (Sec. VI).

II. ORDER PARAMETER OF THE FILM

The *order parameter of the film* is the **c** director, defined as the projection of the molecular director **n** onto the smectic layers [Fig. 1(b)]. Due to the vicinity of the free surface, the director **n** is not equivalent to $-\mathbf{n}$. It is therefore a real vector, as also its projection **c** onto the smectic layers. The polar symmetry of the film arises from the asymmetry of the film itself, combined to the molecular tilt, in a mechanism that is different from the one discovered by Meyer in the chiral SmC^* liquid crystals [24]. The polar property of the surface-induced films is a surface property that vanishes in the bulk of the film, a few smectic layers below the free surface. There, **n** and **c** should again become equivalent to their opposite as usual [2].

Several physical mechanisms are able to produce a surface electric polarization. Two chemical systems in contact, as air and liquid crystal, have naturally different electronic affinities. They consequently exhibit different electric poten-

tials, and an electric field appears at their interface, which in turn, induces a permanent electric polarization. Other mechanisms may add up their effects, as the ordoelectric [25] or flexoelectric effects [26,27]. In both cases, an electric polarization is produced by means of gradients in the orientational order close to the surface. For symmetry reasons, these gradients are perpendicular to the surface. In the ordoelectric case, the polarization results from gradients of the orientational order parameter S, while in the flexoelectric case it is due to gradients in the average tilt angle of the molecules; indeed, such tilt variations in the interfacial smectic layers of the surface-induced films have been observed by means of careful birefringence measurements [28]. When the molecules are tilted in the film, as here, the electric polarization is tilted too. In our setup, (see below), we can apply an electric field **E** horizontally onto the film, by means of electrodes evaporated on the glass substrate (Fig. 1). In the following, we therefore restrict our attention to the projection of the polarization onto the film, **P**. Both vectors **P** and **c** are therefore parallel to each other, and attached to the free surface of the film.

In previous experiments, we were able to estimate the horizontal component of the surface polarization **P** in 1-(methyl)-heptyl-terephthalidene-bis-amino-cinnamate (MHTAC) surface-induced films by means of a measurement of its ratio over the average Frank elastic constant $\mathcal{K}$. On taking the estimate $\mathcal{K}\sim 5\times 10^{-12}$ N, known to be valid for standard nematic liquid crystals, we deduced $P\sim 4\times 10^{-14}$ C/m [16,29]. However, as shown later, the equivalent Frank elastic constant in tilted smectics is about two orders of magnitude larger than in nematics. In particular, the smectic splay elastic constant has been directly measured in the SmC^* phase of 2-methylbutyl 4-(4′-n-decyloxybenzylidene amino)-cinnamate (DOBAMPC) to be worth $K_s\sim 6\times 10^{-18}$ J per layer [30]. We therefore have to correct the above elastic and electric estimates by a factor of about 200, so that we deduce, in particular, that $P\sim 10^{-11}$ C/m. Let us note that this last value is consistent with the estimate obtained on the basis of a flexoelectric effect [27] and on assuming an overall tilt variation across the film of the order of 1 rd. Though the evaluation of the projected polarization per surface unit of the MHTAC film seems small, it is nevertheless much larger than a typical ferroelectric polarization per smectic layer, $P^*\sim 10^{-13}$ C/m, as measured for instance in the smectic C^* ferroelectric phase of DOBAMBC [30].

Due to their asymmetry, our films bear a surface electric polarization **P** parallel to **c** [16], and a space charge density $-\boldsymbol{\nabla}\cdot\mathbf{P}$. These electric charges, however, have no practical consequences if their interaction energy $P^2q/8\varepsilon$ is small compared to the elastic energy of the film, Kq^2, $K\sim\mathcal{K}Nd$ being the 2D average elastic constant of the film, N being the number of smectic layers in the film, and $d\sim 3$ nm being the layer thickness. With the above data, we have $K\sim N\times 4\times 10^{-18}$ J and $P\sim 10^{-11}$ C/m. We thus deduce that the electric effects are negligible if the wave-vectors involved in the distortion are larger than $q>N^{-1}\times 10^5$ m^{-1}, i.e., if the wavelength of the distortion is smaller than $N\times 40$ μm. As we shall see below, this condition is fulfilled in the useful range of our experiments. So, in the following, we neglect the electric effects in the MHTAC surface-induced film and we restrict our attention to the elastic properties.

The free energy of the film may therefore be expanded in terms of the lowest order invariants that may be built with the order parameter **c** and its gradients. They respectively yield the Landau and Landau-Ginsburg energies, the latter terms corresponding physically to an elastic energy, since they directly involve the distortion through the **c** gradients. Due to the two dimensional nature of the film, there are only two *quadratic* gradient terms. They are classical. Here, because of the reduced symmetry of the system, a supplementary invariant, that is proportional to $\boldsymbol{\nabla}\cdot\mathbf{c}$, i.e., *linear* in the **c** gradient, adds up to the free energy. Formally, this extra term should not be considered as an elastic term, since elasticity is essentially quadratic. It exists because the order parameter of the film, **c**, being a real vector, $\boldsymbol{\nabla}\cdot\mathbf{c}$ is a scalar that keeps invariant upon any axis reversal. However, as noted a long time ago [2], the simplest term to be thought of, $\boldsymbol{\nabla}\cdot\mathbf{c}$, is a total derivative that readily integrates to boundary terms. If the film contains defect lines, this term effectively contributes to the total energy, as discussed in Refs. [19,20]. In defect-free systems, the first invariant term, linear in the distortion, that may be considered is therefore $K_1\mathbf{c}^2\boldsymbol{\nabla}\cdot\mathbf{c}$. Such a term was introduced some years ago by Selinger *et al.* [21] to analyze instabilities in Langmuir monolayers. However, the instability that these authors considered was somewhat different from the one studied here, since it corresponded to small undulations of the **c** field, instead of the continuous rotation of the **c** director that we observe in the surface-induced films [22]. Let us also notice that a similar term, the ferroelectric polarization **P** replacing **c**, was introduced by Jacobs *et al.* [23] for studying instabilities in free-standing films of chiral SmC^*. Again, the instability is rather different from the one discussed here. In particular, it contains arrays of defect lines, very similar to the defect structures studied in Refs. [19–20].

A direct consequence of the $K_1\mathbf{c}^2\boldsymbol{\nabla}\cdot\mathbf{c}$ term is to provide a different energy to the splay distortions according to their sign. In such a system, the positive and negative splay distortions are no longer symmetric. Characterized by different stiffnesses, they should extend differently if they are in competition in the same film, and if therefore they are submitted to the same orientational pressure. Moreover in some cases, $K_1\mathbf{c}^2\boldsymbol{\nabla}\cdot\mathbf{c}$ may be strongly negative so that the whole energy of the film becomes negative. Then, surprisingly, the distorted film exhibits a lower energy than the uniformly oriented one. This means that an instability takes place in the film, for purely elastic reasons.

Clearly, the energy term $K_1\mathbf{c}^2\boldsymbol{\nabla}\cdot\mathbf{c}$ plays a role only if it does not integrate to boundary terms. This condition requires that $\mathbf{c}^2$ not be a constant over the entire surface of the film, and consequently, that the tilt angle of the molecules in the layers undergoes variations, so that the modulus of the order parameter $|\mathbf{c}|$ varies too. Consequently, the Landau energy is involved in this problem, and the effects of the $K_1\mathbf{c}^2\boldsymbol{\nabla}\cdot\mathbf{c}$ term are increased if the tilt modulations are easy, in particular if the sample is close to a real, or virtual, smectic A phase transition. Let us finally notice that linear energy terms in $\boldsymbol{\nabla}\times\mathbf{c}$, since they change sign in a mirror symmetry, are not

invariant in achiral systems. We therefore do not consider them here.

Gathering the invariant energy terms discussed above, we may therefore write the free-energy density per surface unit of the film as [31]

$$f=\frac{1}{2}K_s(\boldsymbol{\nabla}\cdot\mathbf{c})^2+\frac{1}{2}K_b(\boldsymbol{\nabla}\times\mathbf{c})^2 + K_1\mathbf{c}^2\boldsymbol{\nabla}\cdot\mathbf{c}+\frac{1}{2}a\mathbf{c}^2+\frac{1}{4}b(\mathbf{c}^2)^2. \quad (1)$$

In this expression, K_s and K_b stand for the 2D splay and bend, elastic constants of the film, respectively, K_1 is the linear splay elastic constant introduced above, and a and b are the first coefficients in the Landau expansion, also written per surface unit of the film. Except for the term $K_1\mathbf{c}^2\boldsymbol{\nabla}\cdot\mathbf{c}$ which arises from a surface effect as discussed above, all the other contributions to the free energy originate from the film volume. Their respective coefficients are therefore proportional to the film thickness $N\times d$, N being the number of the smectic layers in the film and d their individual thickness, while K_1 should keep independent of N. Formally, K_s and K_b are constants that arise from the Landau-Ginzburg theory. They should therefore be independent of the order parameter $\mathbf{c}$. However, they are currently expressed in terms of the 3D Frank elastic constants and of the molecular tilt angle θ $(=\sin^{-1}|\mathbf{c}|)$. In the following, we replace K_s and K_b by more convenient parameters, the average elastic constant $K=(K_s+K_b)/2$, and the elastic constant difference $\delta K=(K_s-K_b)/2$, or the elastic anisotropy coefficient $\Delta=-\delta K/4K$. As shown earlier, the elastic constant difference δK in tilted smectics is large, of the order of $2K/3$. In particular, we have measured that $\Delta=-0.147\pm0.005$ in 20-smectic-layer-thick, surface-induced films of MHTAC [32]. It is therefore not justified to neglect the elastic anisotropy here, though such an assumption is commonly admitted in the literature, and would clearly simplify the calculations.

III. EXPERIMENTS

Prefreezing films of smectic liquid crystals appear at the free surface of droplets heated up to a temperature slightly above the smectic to isotropic phase transition. We are therefore restricted to work with compounds that exhibit such a direct phase transition from the isotropic to the smectic phase, where, moreover, as discussed above, the molecules are tilted inside the layers.

A. Experimental background

The experiments that we report here are essentially performed with the symmetric mixture of 1-(methyl)-heptyl-terephthalidene-bis-amino-cinnamate (MHTAC), $1/2\,RS+1/4\,SS+1/4\,RR$. This liquid crystal exhibits a SmC_A phase, initially called SmO [33], with *alternate* tilting of the molecules from one layer to the next (as first really shown in Ref. [16]). At 158 °C, the smectic phase directly melts into the isotropic phase. It thus provides the opportunity to observe prefreezing films with tilted molecules inside the layers as required for our study. Moreover, it has several advantages that help in performing the experiments. In particular, it allows one to tune the thickness of the films rather easily, just on changing temperature. With the other liquid crystal compounds that we have tested [18], the surface-induced films do not exceed a few layers. If we try to increase their thickness by slightly decreasing the temperature, we observe that the whole isotropic droplet suddenly freezes into a disordered smectic phase, and destroys the surface-induced film. On the wetting point of view, this means that the surface-induced film is a prewetting film and that it incompletely wets the isotropic phase. It then breaks out at a first order prewetting transition. Conversely, with MHTAC, the prewetting transition is almost second order, or, in other words, close to a critical point. Another advantage of MHTAC is its exceptionally large birefringence. The path difference per smectic layer in normal incidence, $\delta_0=\Delta n d\sin^2\theta\sim0.5$ nm [28], allows one to observe the film in transmitted light by means of a polarizing microscope (Fig. 2). With the polarizers crossed at $+\pi/4$ and $-\pi/4$ from the reference axis, and for very thin films, i.e., for path differences small compared to the wavelength of light, the light intensity is simply expressed as

$$I\sim\delta_0^2N^2(1+\cos 4\phi), \quad (2)$$

N being the number of the smectic layers in the film, and ϕ the azimuthal angle of the director $\mathbf{c}$ referred to the $\mathbf{y}$ axis. In

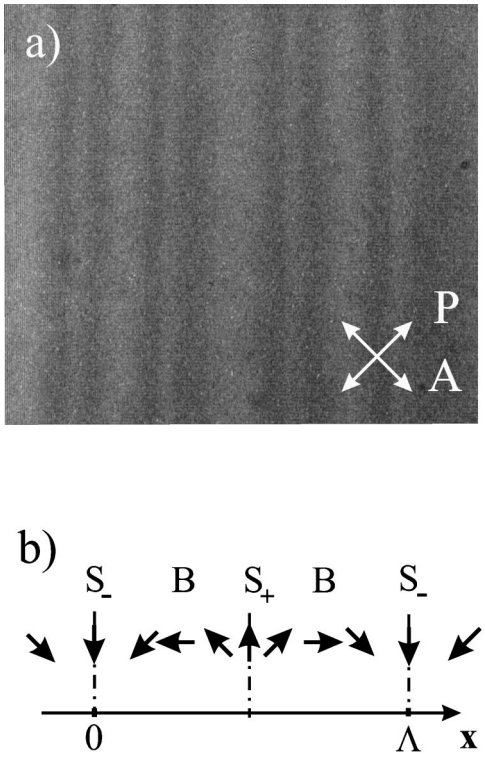

FIG. 2. (a) Spontaneous distortion in a surface-induced film of MHTAC with $N=3$ smectic layers. The polarizers are crossed and oriented at $\pi/4$ from the wave-vector direction. The width of the photograph is about 0.5 mm. (b) Sketch of the **c** coiling up. The dashed lines mark the mirrors of symmetry of the distortion. The widths of the bend, positive splay, and negative splay zones are denoted as B, S_+, and S_-, respectively. Note that conversely to the $N=2$ case, $S_+<S_-$. (see Sec. V C).

this expression, we have neglected the reflections at the film interfaces. Taking the optical indices into account, we estimate the secondary rays to be less than 10^{-4} weaker than the directly transmitted ray, and therefore that any Fabry-Perot effect may be neglected here. The major optical consequence of the film interfaces that we may suspect, is the difference that they introduce between the amplitudes of the two polarizations, parallel and perpendicular to **c**. It is, however, easy to show that this effect is equivalent to an uncrossing of the polarizers by $\Delta n/40 \sim 5 \times 10^{-3}$ rd, and that it may be neglected too.

On measuring the light intensity along the wave vector **q** of the distortion, and using expression (2), we both deduce the number N of the layers in the film and the orientation of **c** modulo $\pi/2$. In order to get the complete determination of ϕ, we take into account that the director **c** is parallel, in the same sense, as the electric polarization **P**. On briefly applying an electric field **E** in the plane of the film, and on noticing the places that suddenly extend (which means that they have the lowest electric energy), we determine where **P**, and therefore **c**, is parallel in the same sense as **E**. This observation, combined with the continuity of the **c** field, allows us to get the exact determination of ϕ everywhere in the film. Let us mention here that we prefer sometimes to determine N independently just by counting the number of simple dislocations, or steps, that pass across the observation field when cooling down the sample from a temperature ($\sim$165 °C) high enough for the film be completely melt.

To generalize our results, we have performed similar experiments on other liquid crystals too. Except with hexadecanoxybenzoic acid (16O*BA*), the surface-induced films keep very thin and reach a maximum of one or two layers only [18]. They are therefore extremely difficult to observe and to measure. With 16O*BA*, the film is five layers thick at the transition to the isotropic phase (133 °C). It is then in the smectic *C* phase, with all the molecules being tilted in the same direction. Unfortunately, the path difference per smectic layer is small in 16O*BA*, partly because of a comparatively smaller tilt angle $\theta \sim 43.5°$ [34], instead of $\theta \sim 50°$ for MHTAC [33]. The accuracy of the optical measurements is therefore rather poor, so that the results with this compound only keep qualitative [22].

The experimental set-up is simple, and has been described elsewhere [22]. A puddle of MHTAC, a few micrometers thick, is placed on a glass plate, and is accurately thermocontrolled by means of an INSTEC card, slightly above 158 °C, the isotropic to SmC_A phase transition. The film is observed in transmitted light with an Orthoplan Leica microscope. The parasitic birefringence of the whole setup, including the windows of the thermostat, is almost uniform in the field of observation, smaller than 0.5 nm. The pictures are caught by means of a high-sensitivity Cohu video camera, digitized with a Matrox IP-8 card, and accumulated in a microcomputer. In this manner, the noise that is inerrant to our low light conditions, is partly washed out, and the images that we get, are correct enough for light intensity analyses along an **x** axis perpendicular to the spontaneous distortion, i.e., parallel to its wave vector **q**.

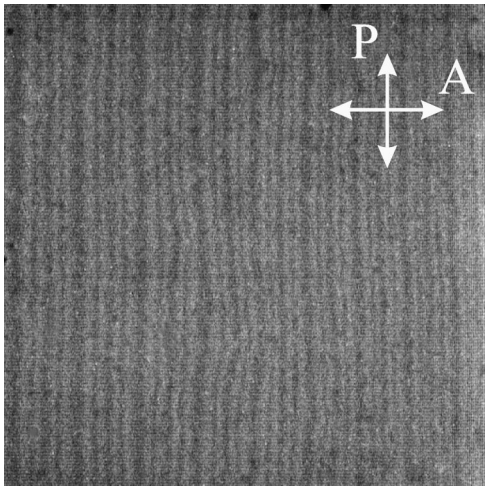

FIG. 3. Spontaneous distortion in the same film with about the same magnification as in Fig. 2a, but now the polarizers are parallel and perpendicular to the wave vector of the distortion, to give better evidence of the four-fringe period.

B. Observations

Typical photographs of a three-layer-thick film are shown in Figs. 2 and 3, with the polarizers respectively oriented at $\pi/4$ and 0 rd, modulo $\pi/2$, from the **x** axis. The film shown in Fig. 2(a) exhibits a distortion of the **c** director field with a relatively large period $\Lambda = 2\pi/q \sim 250$ μm. Its smooth appearance clearly indicates that it does not contain any disclination lines, contrary to the case discussed in Ref. [19]. This fact is even more striking when observing the film on rotating the microscope stage. The stripes then just drift along the **x** axis. This observation indicates that the structure of the distortion corresponds to a continuous rotation of the **c** director along the **x** axis, as sketched in Fig. 2(b) [and modeled in Eq. (3)]. It thus forms an array of disclination walls, with alternate splay and bend distortions. Since the compound is achiral, the structure exhibits mirrors of symmetry, perpendicular to the **x** axis and located at a distance $\Lambda/2$. The bend distortions along the **x** axis are therefore equivalent and independent of the sense of rotation. Conversely, the splays depend on the sign of $\nabla \cdot \mathbf{c}$. The widths of the distortions, measured between the places where the **c** director is oriented at $\pi/4$, modulo $\pi/2$, from the wave vector **q**, i.e., between the black fringes (Fig. 2), are called B, S_+ and S_-, respectively for the bends, positive splays and negative splays. The period Λ of the distortion therefore corresponds to four fringes, though this is not absolutely evident on the photograph of Fig. 2(a). It is easier to observe that the period effectively corresponds to four fringes for smaller periods if the polarizers are rotated by $\pi/4$, i.e., parallel and perpendicular to the wave vector **q**. See, for instance Fig. 3, where $\Lambda \sim 50$ μm. The texture again appears to be free of disclination lines. This point is therefore independent of the period of the distortion, as far as it is possible to see.

The distortion comes spontaneously up when cooling down the film, a few degrees above the melting temperature to the isotropic phase [22]. At the beginning, the film is one layer thick ($N=1$) but the stripes are already there, faint and

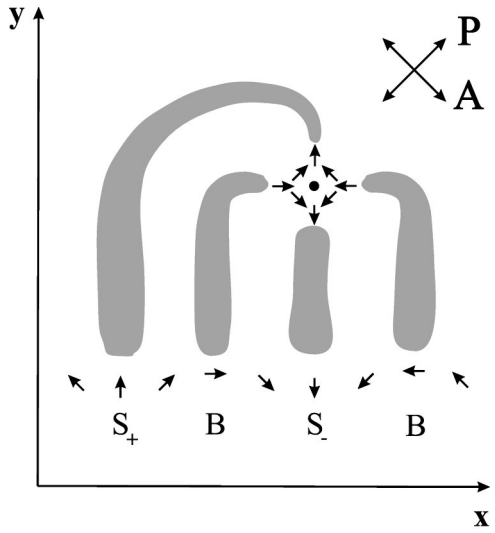

FIG. 4. Sketch of a -1 point defect in an $N=2$ surface-induced film, as observed between polarizers crossed at $\pi/4$ from the **x** axis, chosen parallel to **q**, the **y** axis being oriented towards the droplet center. The defect is close to an island of impurities located upwards, out of the figure, and drives a right-handed distortion wall ($q<0$). The black fringes are depicted as gray zones.

loose. Both the film and the disclination walls appear continuously. At that moment, the walls are broken in bars with disclination point defects of opposite strengths, $+1$ or -1, at both ends. On slowly cooling again, the point defects move towards an edge or towards the droplet center according to their sign. The $+1$ defects are finally rejected out of the film, probably because of a too heavy energy cost, while the -1 point defects gather close to an island of impurities floating around the summit of the droplet. In their movement, the disclination walls are dragged and elongated, getting denser and roughly parallel to one another, and they finally draw a radial figure over the whole droplet. This process imposes a unique coiling sense for the distortion that precisely corresponds to the right-handed **c** rotation when moving in the **x**-axis direction (i.e., $q<0$), this axis being oriented in such a way that the **y** axis points towards the droplet summit, i.e., towards the floating island (Fig. 4). In this manner, the wall and the -1 point defect both involve local distortions of negative q wave-vectors that may adapt easily to each other through weak supplementary distortions. The elastic energy of the film may then be minimized a little bit further on placing the -1 point defects along the narrowest splay walls (that correspond to negative splays in the case of a two-layer-thick film, as sketched in Fig. 4).

On decreasing the temperature again, but not so as to increase the film thickness, we observe that the walls get stiffer and more contrasted and finally build up a regular array of distortions, as shown on the photographs of Figs. 2 and 3. Their energy is negative compared to the energy of a uniformly oriented film since they appear spontaneously. From time to time we observe new walls that grow up in the film and decrease the period Λ of the distortion. However, the wall nucleation is difficult, and indeed, becomes more and more exceptional as temperature is lowered. The nucleation occurs at the edge of the film which, in fact, is a triple

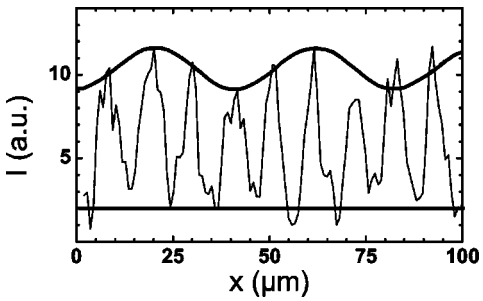

FIG. 5. Light intensity measured as a function of the distance x along the wave vector of the distortion **q** in a surface-induced film of MHTAC, two smectic layers thick. The film is placed between polarizers crossed at $\pi/4$ from **q**. The light intensity variations and its envelope are shown by means of a thin line and heavy lines, respectively. The interference fringes exhibit a typical intensity modulation with a four-fringe period.

line between liquid crystal, solid substrate and the air. In these places, the **c** director is anchored onto the solid substrate, and so the corresponding energy has to be activated for the nucleation process may take place. Clearly, the distortion does not coil up thoroughly, the film never reaching its complete equilibrium. This explains the wide spread values that we observe for the period Λ of the distortion.

On cooling down temperature further, an edge-dislocation line passes at the film interface with the isotropic droplet [35]. The film thus gets a new smectic layer and its thickness increases ($N=2$). Then, and for thicker films, we observe that walls may retract and eventually disappear into the film edge, now increasing Λ. This observation shows that, for $N>1$, the film energy becomes positive, compared to the undistorted state. However, the nucleation process for pinning off walls out of films, two or more layers thick, appears to be much more difficult and exceptional than for creating new ones in $N=1$ films, probably because of a larger anchoring strength at lower temperatures. In practice, the array of disclination walls becomes metastable for $N>1$, and remains frozen in, even if the film thickness is increased up to $N=5$ or more. Most often, disclination walls take the opportunity of a surface edge-dislocation line, or step, that passes across the smectic-isotropic film interface, to disconnect from the edge of the film and then to retract towards the droplet center and disappear.

C. Measurements

Since the distortion never reaches equilibrium, the period Λ is, in fact, a free parameter that widely depends on the experimental conditions and in particular, on the time. From the free energy of the film, that depends on Λ through Eq. (1) one may define a parameter conjugated to Λ. This parameter directly acts onto the orientational periodicity of the distortion. It has therefore the physical meaning of a pressure, and we may refer to it as the orientational pressure.

In Fig. 5 we show the light intensity measured along the **x** axis, perpendicular to the stripes, on a surface-induced film of MHTAC, two smectic layers thick, the film being placed between crossed polarizers, respectively rotated by $+\pi/4$ and

$-\pi/4$ from the **x** axis. In order to filter out a large part of the noise that pollutes the images (Figs. 2 and 3), we perform a space-time data accumulation over 32–64 rows of pixels parallel to the **x** axis, on typically 100 video frames. In the case that the period, which corresponds to four fringes, is short as in Fig. 5 ($\Lambda=42$ μm), we then clearly observe a modulation of the interferences. This is a direct indication that the tilt of the molecules, and therefore the **c** modulus, changes along the **x** axis. At large periods, i.e., at small q's, the light modulation becomes difficult to detect out of the experimental noise. With thinner films ($N=1$), the birefringence is about twice as smaller, so that the signal to noise ratio is decreased by a factor of 4 [Eq. (2)]. The measurements then do not give any useful information. We therefore begin the measurements with $N=2$ films. The noise decreases with thicker films, but simultaneously the modulation also decreases and the measurements are practically useless for N larger than 4.

From light intensity measurements as shown in Fig. 5, we deduce at the same time, the amplitude of modulation of the light intensity and the positive and negative splay widths S_+ and S_-, as functions of q^{-1}. We further use both types of measurements to test the validity of the model that we propose in the next sections to analyze the experiment.

IV. CALCULATION OF THE MODEL

In order to get a better understanding of the spontaneous distortions that we observe in the surface-induced films of tilted smectic liquid crystals, we now try to compare our experimental results, observations, and measurements to the **c** field that minimizes the free energy of the film [Eq. (1)].

A. Fourier expansion

Formally, the periodic **c** field may be expanded as a Fourier series. To write this, we prefer to use the polar coordinates of the **n** director, θ and ϕ, essentially because they are well suited to express the overall rotation involved in the observed distortions. Keeping terms up to the second order only, we have

$$\phi(x)=\omega+\delta\phi_1\sin\omega+\delta\phi_2\sin 2\omega,$$

$$\theta(x)=\theta_0+\delta\theta_0+\delta\theta_1\cos\omega+\delta\theta_2\cos 2\omega, \tag{3}$$

where $\omega=\mathbf{q}\cdot\mathbf{r}=qx$, and where we have taken into account that $\phi(x)$ and $\theta(x)$ are odd and even functions, respectively, due to the mirror of symmetry at $x=0$ [Fig. 2(b)]. This Fourier expansion involves 5 parameters. One would like to reduce this number, but the second order is necessary here because of the strong elastic anisotropy of the tilted smectic phases that we mentioned above. This large anisotropy makes the splay domains to be noticeably larger than the bend ones, and consequently produces large 2ω Fourier components that cannot be neglected.

Let us also note that according to the experimental observations, the spontaneous distortion arises continuously from an array of parallel and periodic, individual disclination walls, or solitons. Clearly, we need a great number of Fourier terms to describe the distortion in the soliton regime, at large q^{-1}. We therefore deduce that the above expansion, when limited up to the second order [Eqs. (3)], cannot be a correct approximation in the very large q^{-1} range. In the following, to avoid this problem, we restrict its use to the range of q^{-1} at least one order of magnitude smaller than the soliton width [36].

B. Theoretical solution

Averaging the free energy density [Eq. (1)], we may now easily calculate the free energy F per surface unit of the distortion approximated in Eqs. (3), up to quadratic terms:

$$\begin{aligned}\frac{4}{b}F=&\,\delta\theta_0^2+\frac{1}{2}\delta\theta_1^2+\frac{1}{2}\delta\theta_2^2-k_1\\&\times\left[\delta\theta_1+\delta\phi_1\delta\theta_2+\frac{1}{2}\delta\phi_2\delta\theta_1+\delta\theta_0\delta\theta_1+\frac{1}{2}\delta\theta_1\delta\theta_2\right]\\&+k\left[\frac{1}{2}+\delta\theta_0+\frac{1}{4}\delta\phi_1^2+\delta\phi_2^2+\frac{1}{4}\delta\theta_1^2+\delta\theta_2^2+\delta\phi_1\delta\theta_1\right.\\&\left.+2\delta\phi_2\delta\theta_2\right]+\delta k\left[\frac{1}{2}\delta\phi_2-\frac{1}{2}\delta\theta_2-\frac{1}{8}\delta\phi_1^2+\frac{1}{8}\delta\theta_1^2\right.\\&\left.+\delta\phi_2\delta\theta_0+\frac{1}{4}\delta\phi_1\delta\theta_1\right],\end{aligned} \tag{4}$$

where we use the dimensionless parameters

$$k_1=\sqrt{2}\,\frac{K_1 q}{b},$$

$$k=\frac{2Kq^2}{b},$$

$$\delta k=\frac{2\delta K q^2}{b}. \tag{5}$$

In the case that the wave vector q is small enough for $k<k_1<1$, and that nevertheless, $k_1^2<k$, which corresponds to being below the threshold of the instability (see below), the minimum of free energy is obtained for a distortion such that

$$\delta\theta_0=-\frac{k}{2},$$

$$\delta\phi_1=-2k_1\left(1+\frac{3\Delta}{2}\right),$$

$$\delta\theta_1=k_1\left(1+\frac{\Delta}{2}\right),$$

$$\delta\phi_2=\Delta,$$

$$\delta\theta_2=\delta k, \tag{6}$$

where the terms of higher orders than k_1, k, and δk have been dropped out, and where, for simplification, the elastic

anisotropy is taken into account at the first order only through the coefficient $\Delta = -\delta K/4K \sim -0.15$. Except for $\delta\phi_2 = \Delta$, which eventually confirms that the Fourier expansion has effectively to be performed up to the second order, all the Fourier coefficients of Eqs. (3) are vanishingly small as q or q^2. Provided that q is not too small to enter into the regime of the periodic solitons, we may anticipate that Fourier coefficients of order larger than 2 are even smaller. This justifies that they are negligible, and that the above cutoff of the Fourier expansion at the second order [Eqs. (3)] is correct.

Let us now convert the dimensionless conditions $k < k_1 < 1$ in terms of experimental quantities. These conditions mean both $q < q_1 = b/K_1\sqrt{2}$ and $q < q_2 = K_1/K\sqrt{2}$. For a two-layer-thick film ($N=2$), with $|K_1/b| \sim 0.5$ μm (see below), we have $q_1^{-1} = 0.7$ μm. We may also rather easily obtain an evaluation of q_2^{-1} if we remember that the two-layer-thick films are close to the instability threshold (Sec. III B). This means that, for $N=2$, the parameters of the film roughly satisfy the condition $K_1^2 \sim Kb$ (see Sec. IV C), and therefore that $q_2^{-1} \sim q_1^{-1} \sim 0.7$ μm. Indeed, these limits are optically below our optical resolution, so that the conditions, $q < q_1$ and $q < q_2$, are experimentally fulfilled here.

In other systems, however, the large-q limit may be easier to reach. Though not valid then the above model allows us to see that the different $\delta\theta$ components should begin to diverge with q and get as large as θ_0 itself at some moment. Then, for particular values of x that correspond to periodic parallel lines, the tilt should get null. In these places, the SmC_A film melts into the SmA phase, forming an array of disclination lines. It thus suppresses the places where the energy involved by the $\mathbf{c^2\nabla\cdot c}$ term is positive. For instance, in the case of two-layer films, $K_1(N=2)$ being negative (see below), the negative splay domains should then collapse, leaving only an array of positive splay domains separated with parallel defect lines. This situation indeed corresponds to the one first proposed in Ref. [19] where, to simplify, the tilt is taken to be constant, and where consequently, the linear splay term just reduces to the $\mathbf{\nabla\cdot c}$ term. Nevertheless, in view of the above q_1 and q_2 estimates, this simplification does not seem to be observable in our films.

C. Free energy minimum

We may estimate the minimum of the film free energy by calculating the free energy per surface unit F_0, that corresponds to the above solution [Eq. (6)]:

$$\frac{8}{b}F_0 = k - k_1^2(1+\Delta). \tag{7}$$

Apart from secondary effects due to the elasticity anisotropy, this expression roughly shows that, for $k < k_1^2$, the minimum of free energy becomes negative, i.e., that the distortion may then occur spontaneously. So, the relation $k \sim k_1^2$, or $Kb = K_1^2$ in terms of experimental parameters, corresponds to the threshold of the instability observed and discussed here.

As mentioned in Sec. III B, walls tend to retract and eventually to disappear in films several layers thick. This observation indicates that, for $N>1$, the instability is unable to develop by itself, and that the film is below the instability threshold. The parameters of the film should then satisfy the inequality $K_1^2 < Kb$, or $k_1^2 < k$, which is a necessary condition for the validity of the solution presented in Sec. IV B.

Finally, the last point to verify, is that the cutoff at the second order of the Fourier series [Eqs. (3)] is effectively valid. As we mentioned in Sec. IV B, this approximation is correct for q^{-1} much smaller than the soliton width, a limitation that may be evaluated simply in view of the experimental results. We therefore do not try here to calculate it in the details [36].

V. DATA ANALYSIS

As noted above, the distortion in our surface-induced smectic films exhibits an unusual four-fringe period that concerns both the azimuthal direction (Fig. 3) and the modulus of the **c** director (Fig. 5). This property is clearly consistent with the above Eqs. (3) and (6), and therefore with the existence of a linear elastic term $K_1\mathbf{c^2\nabla\cdot c}$ in the film free energy. In order to test the experiment and the proposed model further, we have to perform quantitative comparisons. To this aim, we extract physical quantities from the light intensity measurements, that may be rather easily compared to the model, as the amplitude of tilt modulation, and the widths of the positive and negative splay domains, S_+ and S_-.

A. Splay widths in films two layers thick

The **c** direction being determined on briefly applying a small electric field in the plane of the film (Sec. III A), we first deduce the signs of the different splay domains in the distortion field. We then measure their width from the distance between the black fringes that border them when the polarisers are crossed at $\pi/4$ from **q**. We repeatedly perform these measurements for different periods Λ, and different numbers of smectic layers in the film N.

In Fig. 6(a) are shown the measurements of S_+ and S_- as functions of $q^{-1} = \Lambda/2\pi$ in a two-layer-thick film, with open and close dots, respectively. Both quantities are clearly different at large periods, since S_- saturates around 50 μm, while S_+ continues to grow with Λ. They thus exhibit a dissymmetry that confirms the four-fringe period mentioned above. At small Λ, however, the two splay widths get close to each other, and eventually seem to become identical. A data analysis, as we propose now, is necessary to clarify if a difference really persists between the two splay widths.

From Eqs. (3), (5), and (6) and under the same conditions as to obtain them, we may estimate

$$S_\pm = \left(\frac{\pi}{2} - 2\Delta\right)\frac{1}{q} \mp \frac{4K_1}{b}\left(1 + \frac{\Delta}{2}\right). \tag{8}$$

Though the coefficient $\delta\phi_2$ keeps constant and equal to the elastic anisotropy coefficient $\Delta \sim -0.15$, and therefore cannot be neglected in any expansion, the main limitations to this approximation essentially come from the validity conditions needed for the second-order Fourier expansions (3). As discussed in Secs. IV A and IV C, this condition limits the

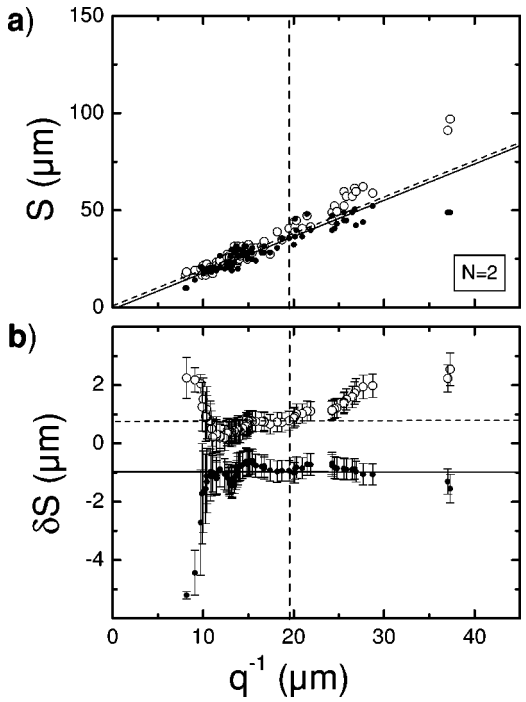

FIG. 6. (a) Widths of the positive and negative splay domains, S_+ and S_-, as functions of $q^{-1}=\Lambda/2\pi$ in a two-layer-thick film. They are shown with open and close dots, respectively. (b) Differences δS between the splay widths obtained from the fits of Eqs. (8) and the average value S given by Eq. (9) as functions of the cutoff q^{-1} above which the experimental data are rejected out of the fit (see the text). δS_+ and δS_- are shown, with their calculated standard deviations, as open or close dots according to they originate from the S_+ or S_- measurements, respectively. Away from the vertical long-dashed line, i.e., for q^{-1} larger than ~ 20 μm, the crossover begins to deviate the data noticeably from the model. Below this limit, the model is valid. The best fitted value of K_1/b is therefore obtained for cutoffs around 20 μm, where the standard deviations are minimum. The best fits are shown in both (a) and (b), as short-dashed and solid lines for the positive and negative splays, respectively.

range of validity of our model to q^{-1} being much smaller than the soliton width that we may estimate now to be of the order of the saturation value of S_-, i.e. $q^{-1}\sim 50$ μm. This distance therefore marks the separation between two regimes, a small q^{-1} regime that may be described with the above model, and a soliton regime for larger q^{-1}. In between, a crossover extends continuously over an undetermined region. We therefore cannot analyze the experimental data of Fig. 6(a), directly on fitting expressions (8) onto them. We have to eliminate from the fit the data that belong to the crossover domain. To determine the crossover extension, we perform different fits on a restricted basis, by rejecting the experimental data of larger q^{-1} than a given cutoff. We then progressively reduce the chosen cutoff, and we observe the way the parameters of the fit evolve. At first, they continuously drift due to the crossover effect, and they finally stabilize when the fitting domain gets out of the crossover region. At that moment, the crossover action becomes negligible compared to the experimental errors, and the fit may be considered as correct. With this method, we test the validity of the model and we are able to determine its physical parameters.

Practically, we proceed in two steps. Noticing that the S_+ and S_- data are in equal numbers for each q^{-1} value, we average Eqs. (8) over both signs of splays, to

$$S=\left(\frac{\pi}{2}-2\Delta\right)q^{-1}, \tag{9}$$

and first we fit this expression of the average splay width versus q^{-1} onto the experimental data taken as a whole, on mixing both S_+ and S_-. This fitting appears to be rather stable and resistant to the crossover effects, since the S_+ and S_- deviations partly compensate for one another. With the data of Fig. 6(a), we thus find the elastic anisotropy coefficient $\Delta=-\delta K/4K=-0.15\pm 0.01$, a value that is consistent with a previous determination [32].

In a second step, we fix Δ at the previously determined value, -0.15, and we perform separate one-parameter fits of the linear equations (8) onto the experimental data, S_+ and S_-, respectively. The fits are performed independently for both signs of splays, on applying again the stability procedure detailed above, i.e., on eliminating the data above a specific cutoff q^{-1}. For each cutoff q^{-1}, the fitted parameter yields the corresponding offset $\delta S=(4K_1/b)[1+\Delta/2]$ from the average splay width S [Eq. (9)]. In Fig. 6(b) we plot δS versus its cutoff q^{-1} with its calculated standard deviation, as an open or a closed dot according to whether it originates from the S_+ or S_- measurements, respectively. Clearly, the two types of data, concerning the positive and negative splays, are now well separated whatever the value of q^{-1}. This result was not clear initially on the raw data plot of Fig. 6(a). This is interesting since it shows that the offset δS is not restricted to the soliton regime where nonlinear effects may take place. Clearly, it persists in the region below $q^{-1}\sim 20-25$ μm, where the crossover effects disappear within the standard deviations, and where therefore, the validity conditions of the above calculations (Sec. IV) are fulfilled. At very small q^{-1}, below 10–12 μm, the number of data that enter into the fit become so restricted that the standard deviation strongly increases and correlatively, the fitted values are more and more dispersed [Fig. 6(b)]. Between these two limits, the fitted δS_+ and δS_- are rather stable around values, respectively, marked by dashed and solid lines:

$$\delta S_+=0.78\pm 0.34 \ \ \mu\text{m},$$

$$\delta S_-=-0.93\pm 0.36 \ \ \mu\text{m}. \tag{10}$$

At first sight, the standard deviations obtained here from our fitting procedure seem unreasonably small in view of the relatively poor quality of our light intensity measurements (Fig. 5), though we get them after a large data integration (Sec. III C). In fact, the fitted parameters (10), δS_+ and δS_-, result from another two-stage data accumulation. First, the raw data in Fig. 6, i.e., the splay widths S_+ and S_-, are extracted from the intensity profiles through a direct averag-

ing over several periods. They are thus obtained to within an accuracy of 2–3 micrometers. Then, the fittings of Eqs. (8) (Fig. 6) are performed on about 40 to 50 data each, so that the resulting standard deviations on the fitted parameters, δS_+ and δS_-, are again reduced by a factor of 6–7.

Remarkably, the fitted offsets (10) have opposite signs, but the same modulus within the standard deviations, as in the model proposed above [Eqs. (8)]. They respectively yield K_1/b values, $K_1/b=-0.68\pm0.29$ μm and $K_1/b=-0.81\pm0.32$ μm, that are consistent with one another within the standard deviations. In order to test the stability of the results relative to the lowest q^{-1} data, we proceed similarly as for large q^{-1}, and we perform successive fits on progressively suppressing the experimental data from the small q^{-1} side. We observe that the fittings keep about stable inside increasingly large standard deviations. Such a behavior is normal since less and less data are taken into account in the fit. It also indicates that the results of Eqs. (10) suffer no particular bias, and that the corresponding values of K_1/b may be considered as correct. Taking the average between these two values, we get $K_1/b=-0.75\pm0.30$ μm for a two-layer-thick film of MHTAC. This value is of the order of magnitude as a previous evaluation based on the same model [31]. The difference from this earlier evaluation, about 35% smaller, essentially comes from the manner that the approximations were taken in the calculation. In Ref. [31], only ϕ was expended in a Fourier series, while θ was just considered as a variable coupled to ϕ. This approach was simpler than the one presented here, since it needed three parameters instead of five but it came to force $\delta\theta_0$ and $\delta\theta_2$ to be zero. In this manner, first order errors were irremediably introduced in the calculation of Ref. [31].

Let us finally note that, since the elastic anisotropy coefficient Δ is a constant ($\Delta=-0.15$), the calculation at the first order in Δ proposed here, could seem questionable. In fact, as may be seen in Eqs. (8), the resulting relative errors on δS_+ and δS_- are of the order of Δ^2, i.e. of a few percent, which is fairly acceptable.

B. Amplitude of the tilt modulations

As Eq. (2) shows, the intensity of the interference fringes is proportional to $\sin^4\theta=\sin^4\theta_0[1+4\delta\theta/tg\theta_0]$, i.e., to $1+4\delta\theta$. So, according to the above model, the light intensity of the fringes is modulated by the molecular tilt variations $\delta\theta=\delta\theta_0+\delta\theta_1\cos\omega+\delta\theta_2\cos 2\omega+\cdots$, and therefore, has the same phase as ω. In other words, the intensity modulation of the interference fringes exhibits the same phase as the fringes themselves. Though our light intensity measurements are a bit noisy, we easily verify this simple property, e.g., in Fig. 5.

Let us now test the model further. As Eqs. (6) show, the second order term $\delta\theta_2$ is small compared to $\delta\theta_1$. So, and taking the low accuracy of our light intensity measurements into account, we are not able to estimate it here. We only can determine the amplitude $\delta\theta_1$ of the tilt modulations for the smallest periods Λ, the measurements becoming worse at large periods because, as may be seen in Eqs. (5) and (6), $\delta\theta_1$ decreases with q, and quickly becomes smaller than the noise. This explains that our tilt measurements are restricted to a smaller q-range than the splay widths.

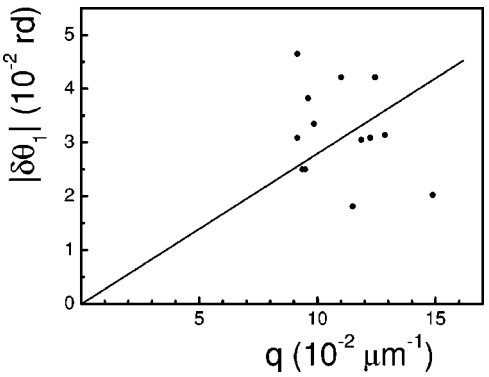

FIG. 7. Modulus of the tilt modulation as a function of q in a two-layer-thick film. A best fit of the theoretical q variations yields a third independent determination of the ratio K_1/b (see the text).

In Fig. 7 we plot the amplitude of the tilt modulation as a function of q in a two-layer-thick film. The data appear to be rather dispersed, and it is clearly impossible here to test the q-dependence predicted in Eqs. (5) and (6). We may nevertheless admit the linear variations of $\delta\theta_1$ with q, and deduce the proportionality coefficient. In this way, we get a supplementary measurement of the ratio $|K_1/b|=0.79\pm0.08$ μm in a two-layer-thick film of MHTAC, that is clearly independent of the previous determinations obtained from the splay widths. Note that we do not obtain the sign of K_1/b here, since our method for determining the sense of the **c** director does not apply for the small periods Λ. This is due to a slow drift that occurs in the film when applying an electric field, and that makes it difficult not to confuse the positive and negative splay domains when the fringes are tightly close.

Let us emphasis that this measurement of K_1/b, which is based on the tilt modulations, is consistent with the two previous determinations, that were independently based on the positive and negative splay widths. Moreover, though the experimental data seem to be of relatively poor quality, they reveal to yield an even better standard deviation on the final result.

C. Films more than two layers thick

Upon slowly decreasing the temperature, single edge dislocations pass at the isotropic-film interface and increase the thickness of the film, layer after layer [18]. As mentioned in Sec. III B, distortion walls may then take the opportunity to untether from the film edge, retract, and eventually vanish, indicating that the distortion is metastable for $N>1$.

We have performed measurements of the splay widths of the frozen-in distortions in films three and four layers thick, as for $N=2$ (Sec. V A). They are shown in Figs. 8 and 9, respectively. The optimum accuracy is obtained for $N=3$, since the path difference is sufficient then to reduce significantly the noise of the light intensity measurements, while the rigidity of the film is small enough not to mask the subtle surface effect of the K_1 term. For thicker films, the measurements are more difficult, and in practice, they become useless above $N=4$.

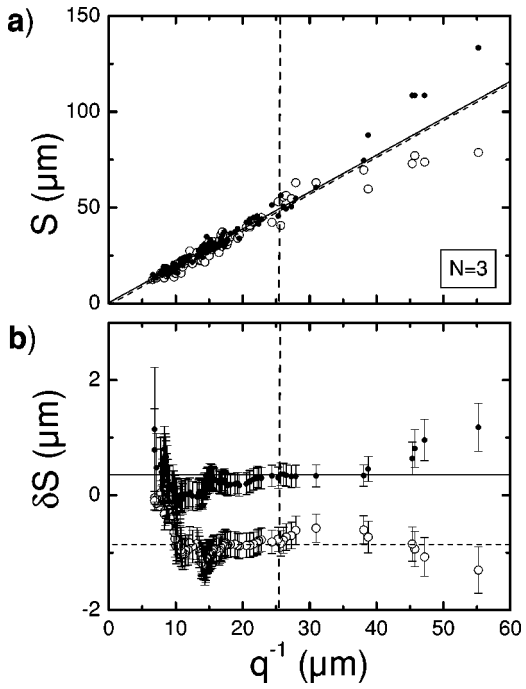

FIG. 8. (a) Widths of the positive and negative splay domains S_+ and S_-, as functions of q^{-1} in a three-layer-thick film (open and closed dots, respectively). (b) Differences δS between the splay widths obtained from the fits of Eqs. (8) and the average value S given by Eq. (9), vs the cutoff q^{-1}, as in Fig. 6. δS_+ and δS_- are shown, with their standard deviations, as open or closed dots according to if they originate from the S_+ or S_- measurements, respectively. For q^{-1} larger than ~ 25 μm, i.e., away from the vertical long-dashed line, the crossover begins to deviate the data noticeably from the model. The best fits are shown in both (a) and (b), as short-dashed and solid lines for the positive and negative splays, respectively.

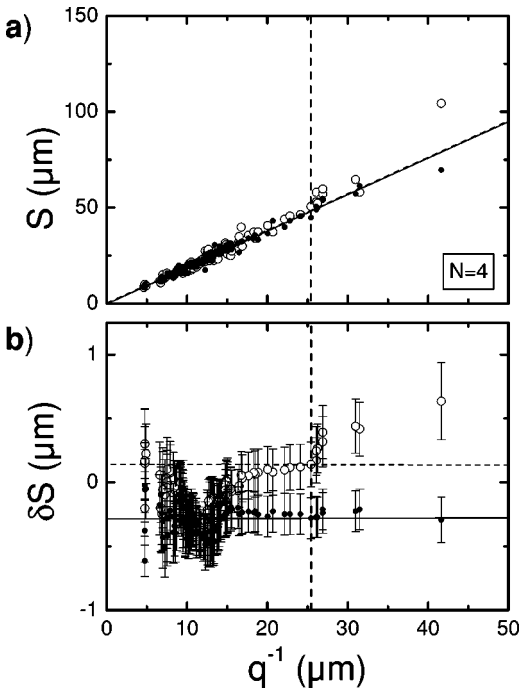

FIG. 9. Same as Figs. 6 and 8, but for a four-layer-thick film. The measurements are taken around $q^{-1} \sim 25$ μm (vertical long-dashed line).

As Figs. 8 and 9 show, the splay widths S_+ and S_- behave similarly for $N=3$ and 4 as for $N=2$. They increasingly separate at large periods, in anticipation to the soliton regime mentioned above. Doing so, they confirm and generalize the observation of distortions with the characteristic four-fringe period, to films thicker than $N=2$. However, we immediately notice that S_+ is alternately larger and smaller than S_-, according to the number of the smectic layers in the film, N, being even or odd. This parity effect is well known in the SmO or SmC_A phase. It gave indeed, the first proof that the molecules in this phase, are alternately tilted at an angle $+\theta$ and $-\theta$ inside the layers, exactly one to one, and not only on average, as macroscopic experiments show [16].

We analyze the experimental data in the same manner as for $N=2$. The crossover effects begin at a slightly larger q^{-1} than for two-layer films, around 25 μm. The best fits are marked in Figs. 8 and 9 as short-dashed and solid lines for the positive and negative splays, respectively. They give independent determinations for the elastic anisotropy coefficient $\Delta = -\delta K/4K = -0.175 \pm 0.005$ for $N=3$, and $\Delta = -0.165 \pm 0.005$ for $N=4$, two values that are consistent with the previous determinations within the standard deviations (see above). More interestingly, they also yield the offsets

$$\begin{matrix} \delta S_+ = -0.84 \pm 0.22 \ \mu m \\ \delta S_- = 0.36 \pm 0.20 \ \mu m \end{matrix} \quad \text{for } N=3,$$

$$\begin{matrix} \delta S_+ = 0.14 \pm 0.18 \ \mu m \\ \delta S_- = -0.28 \pm 0.16 \ \mu m \end{matrix} \quad \text{for } N=4.$$

From these intermediate results, we deduce two independent values of K_1/b separately for $N=3$ and for $N=4$. Taking their respective averages, we obtain the measurements of K_1/b for different film thicknesses. The results are gathered in Table I. They clearly show that K_1/b depends on the film thickness, not only because of the sign, but also for the modulus. These points are discussed in Sec. VI.

As for $N=2$, we measure the light intensity along the wave vector of the distortion in surface-induced films, three and four layers thick. We deduce the amplitude of the corresponding tilt modulations, and get independent determinations of the ratio K_1/b on fitting the linear variations of $\delta\theta_1$

TABLE I. K_1/b ratio deduced from splay width and tilt modulation measurements, for different film thicknesses.

N	$\Delta = -\frac{\delta K}{4K}$	K_1/b (from splay widths)	$\lvert K_1/b \rvert$ (from tilt modulations)
2	-0.15 ± 0.01	-0.75 ± 0.30 μm	0.79 ± 0.08 μm
3	-0.175 ± 0.005	0.51 ± 0.18 μm	0.54 ± 0.09 μm
4	-0.165 ± 0.005	-0.18 ± 0.15 μm	0.17 ± 0.07 μm

with q, according to Eqs. (5) and (6). The measurements are again restricted to the large q range, where unfortunately, we are unable to determine the sign of the splay domains. We therefore only obtain the modulus of K_1/b, with moreover, increasing relative errors (Table I).

VI. DISCUSSIONS

The first striking feature that arises from Table I, is the alternate sign change of K_1/b with the parity of N. The dependence of the physical properties of the surface-induced films on the parity of the number of smectic layers is characteristic of the SmC_A phase, and indeed has been used for the first nonambiguous identification of its phase structure, as recalled above. In particular, this parity effect has been noticed on the textures of racemate SmC_A films observed between crossed polarizers [16], on the orientation of the **c** director with respect to the electric polarization in chiral SmC_A^* films [29], and on the anchoring properties of **c** onto surface edge dislocations [35]. Clearly, it appears every time that, in some manner, a physical effect is involved on the other surface than the one to which the film director **c** is attached, i.e., each time that a physical effect arises from the isotropic-smectic interface. When a smectic layer is added to the film, because of the alternate structure of SmC_A, the isotropic-smectic interface is reverted, and its attached physical effects, too. From the sign changes of K_1/b with the number of layers, we may therefore conclude that the linear elasticity associated with K_1 is essentially localized at the isotropic-smectic interface.

One may nevertheless be surprised that **c** and K_1 are not attached to the same interface. This point may be understood better if we consider that both film interfaces, with the air and with the isotropic phase, formally bear their own surface polarization **P** and their own linear elasticity constant K_1, and that we observe and measure the addition of both polarizations and elastic constants. Practically, only the dominant contributions are observed. They appear to be respectively located at the smectic-isotropic and smectic-air interfaces. Both interfaces thus exhibit opposite efficiencies concerning their electric and elastic properties. Though surprising at first sight, such a behavior is possible essentially because of the completely different origins of the surface polarization **P** and of the linear elastic term $K_1\mathbf{c}^2\boldsymbol{\nabla}\cdot\mathbf{c}$.

The physical meaning of the sign found for $K_1(N)$ may be discussed for a particular film thickness. If we extrapolate the results of Table I, we see that K_1 should be positive in the one-layer case. This sign indicates that at equilibrium the molecules in the smectic layer ''prefer'' to adopt a converging configuration at larger tilts, their tips in contact to the isotropic subphase getting closer to one another, and conversely a diverging splay at smaller tilts. This effect may be understood if one considers that increasing the tilt of the molecules increases the orientational order parameter. Being more ordered, the molecules in the smectic layer reject the disordered molecules of the isotropic subphase more efficiently. They also exert stronger, attractive, van der Waals interactions on the neighboring molecules. Both effects conjugate to bring the tips of the smectic molecules into contact with the isotropic phase closer to one another at large tilts, and thus favor a converging, negative, splay of the **c** director when the tilt is increased. Conversely, in the place of weakly tilted smectic layers, the tips of the molecules in contact to the isotropic subphase should be more disordered and less compact, and should consequently exert a less attractive interaction onto each other. Moreover, a weak tilting favors the intercalations of molecules from the isotropic subphase, again increasing the distance between the tips of the molecules in the smectic layer in contact to the isotropic phase. Both effects thus help to produce a positive **c** splay distortion in the places where the tilt is reduced, as is consistent with the sign found for K_1. Naturally, such a mechanism of molecular intercalation cannot exist at the smectic-air interface. This could explain why the surface-elasticity term in K_1 is only observed at the smectic-isotropic interface of the film.

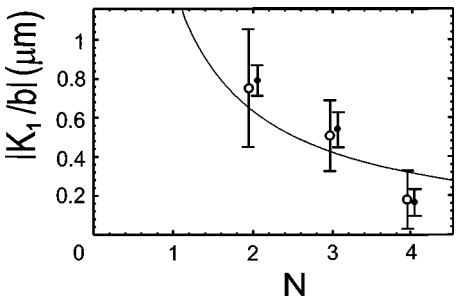

FIG. 10. Modulus $|K_1/b|$ measured as a function of the number N of smectic layers in the film, obtained from splay width (open dots) and tilt modulation (closed dots) measurements. The solid line shows the least-square fit of a hyperbolic law onto the experimental data, $|K_1/b| \sim 1/N$.

Let us now consider the modulus $|K_1/b|$ measured as a function of the number of the smectic layers in the film, N (Table I). It is plotted in Fig. 10. The open and closed dots correspond to the splay width and tilt modulation measurements, respectively. For each N, both types of measurements yield consistent results. This observation is important since both measures are not submitted to the same systematic errors. In particular, an insufficient focusing, or a slight blurring due to the slow drift of the stripes during data accumulation, would lead to an underestimate of the fringe intensities, especially for the thinner fringes. One could consecutively fear systematic errors on the tilt modulation measurements. They therefore appear to be well compensated.

We now examine the variations of $|K_1/b|$ with N. According to the above discussion, K_1 arises from a surface effect, so that its modulus is essentially independent of N. The case of the Landau coefficient b is not so straightforward, and depends on the penetration depth of the tilt modulations that K_1 generates at the isotropic-smectic interface. If the Landau terms are large compared to the elastic energy of a distortion perpendicular to the film, the tilt modulations would practically concentrate on one smectic layer, and the penetration depth would be limited to one layer. The Landau energy would then concern only one layer, as K_1, and the ratio $|K_1/b|$ would be independent of N. As Fig. 10 shows, this hypothesis is not satisfactory. If, conversely, the Landau terms are small compared to the elastic energy of transverse

distortions, the tilt modulations are the same across the whole film thickness. All the smectic layers of the film then involve the Landau energy similarly, so that the coefficient b is proportional to N, and the ratio $|K_1/b|$ is proportional to $1/N$. A least-squares fit of this hyperbolic behavior is drawn as a solid line in Fig. 10. It clearly shows that this second hypothesis of small Landau terms, and uniform tilt variations perpendicularly to the film, is the good one. This means that the anticlinic elastic coupling between layers is strong enough to correlate the tilt variations across the whole film thickness, and to extend the tilt correlation length over a distance larger than a few smectic layers. Indeed, such a property is necessary for the SmC_A phase does really exist.

Though the fit in Fig. 10 concerns only three film thicknesses, it is not excellent, and it passes at the limit of the standard deviations. In fact, things are slightly more complicated than sketched above. The number of smectic layers is experimentally determined on changing the temperature of the whole film, and consequently, K_1 and b, which above have implicitly been supposed to be constant, may change with temperature and, therefore, also with N. This effect could explain the observed deviation from the hyperbolic law in Fig. 10. One may also suspect a superposed deviation due to a parity effect on the modulus of both the parameters b and K_1.

From this least-squares fit, we may nevertheless estimate the one-layer film ratio $|K_1/b(N=1)|=|NK_1/b(N)| \sim 1\ \mu$m, which in turn, allows us to deduce the spontaneous splay constant K_1 itself, provided that we are able to evaluate the Landau parameter b. This evaluation may be done on noticing that the two-layer-thick films are close to the instability threshold (Sec. III B) and that, consequently, the parameters of the film satisfy the condition $K_1^2 \sim Kb$ for $N=2$ (Sec. IV C). So we have $K/b \sim 0.25\times 10^{-12}$ m^2, and taking $K(N=2)\sim 10^{-17}$ J as discussed in Sec. II we both deduce $b(N=1)\sim 10^{-5}$ Jm^{-2} and $K_1 \sim -(-1)^N \times 10^{-11}$ N. We may now try to compare these two quantities to independent evaluations. An order of magnitude of K_1 may be found on considering that the $K_1\mathbf{c^2\nabla\cdot c}$ energy results from local interactions between molecules. With the van der Waals interactions $\sim kT$, and the lateral distance between molecules $l \sim 0.5$ nm, we estimate $|K_1| \sim kT/l \sim 10^{-11}$ Jm^{-1}, which is in good agreement with our measurement. A direct evaluation of b is not possible for the SmC_A phase, where only a few data are available. Instead, we may try to estimate b in the SmC phase, from tilt [37] and tilt susceptibility measurements [38], though this phase is known to be much stiffer than the SmC_A phase. We thus find $b\sim 3\times 10^4$ Jm^{-3} when b is expressed as an energy density per volume unit, or equivalently, $b(N=1)\sim 10^{-4}$ Jm^{-2} if converted per surface unit of a one-layer thick film. This value is an order of magnitude larger than the value measured above in the SmC_A phase, which is in agreement with the observation that the SmC phase exhibits a larger tilt susceptibility than the SmC_A phase [39]. The effect could arise from weaker interlayer interactions in the SmC_A phase, and has been experimentally confirmed by means of easy transitions from the SmC_A^* to the SmC^* phase when applying an electric field.

VII. CONCLUSIONS

Because of their asymmetry, the prefrozen smectic C_A films at the free surface of isotropic droplets of MHTAC exhibit unusual vectorial or polar properties that may have consequences in both the electric and elastic domains, independently. The order parameter that describes the macroscopic properties of these films, i.e., the **c** director, is therefore a real vector. This allows a supplementary invariant, linear in the distortion, $K_1\mathbf{c^2\nabla\cdot c}$, to enter into the free energy of the film, and to significantly change its physical behavior, as to give rise to a spontaneous distortion. In this sense, K_1 may be considered as a *spontaneous splay constant*. The ground state then no longer corresponds to the uniform orientation, but to a continuous rotation of the **c** director, combined to a slight modulation of the tilt of the molecules in the smectic layers. Globally, the distortion may be considered as an array of parallel and periodic walls that moreover exhibit a particular structure, with splay domains of different widths according to the sign of $\mathbf{\nabla\cdot c}$; they therefore exhibit a four-fringe period when observed between crossed polarizers. The period of the distortion cannot easily reach its equilibrium value because, though allowing the system to decrease its energy, each wall has to nucleate from the edge of the film, and this is a slow and difficult process. In practice, the observed periods are not reproducible. They essentially depend on the manner in which the film is produced.

Obviously, the unusual linear invariant term, $K_1\mathbf{c^2\nabla\cdot c}$, introduces a coupling between the Landau energy and the 2D Frank elastic energy of the film, that makes the distortion difficult to calculate exactly. We therefore perform Fourier expansions up to second order (a lower order expansion is not satisfactory since the second order coefficient $\delta\phi_2=\Delta=-\delta K/4K$, which is related to the elasticity anisotropy, is rather large and cannot be neglected). In fact, this analysis significantly differs from the one used in Ref. [31]. In this previous work, based on the same physical model, the mathematical analysis was simplified. Only one variable $\phi(x)$ was expanded in Fourier series up to the second order. The other variable $\theta(x)$ was treated through its first order coupling to $\phi(x)$. Clearly, this approach was not completely satisfactory because it did not use the same order of approximation on the two coupled variables $\phi(x)$ and $\theta(x)$. On the other hand, it needed only three parameters instead of the five here. In fact, the values found by the two methods for the ratio K_1/b, overlap significantly when taking the error bars into account. This is not so much surprising *a posteriori* if we notice that the coupling used in Ref. [31] amounts to drop down the two smallest coefficients, $\delta\theta_0$ and $\delta\theta_2$, that are respectively proportional to k and δk, i.e., that are of order q^2. In both cases, the expansions are not valid at large wave vectors. There, the structure of the distortion is close to a well-known and simpler case with *disclination lines* replacing the splay domains of the disfavored sign, the molecular tilt keeping constant everywhere in the film. The calculation is also limited on the small q side, since there the system evolves towards an array of *solitons* that cannot be described with a Fourier expansion limited to the second order.

We then use this expansion to analyze our optical measurements on the orientation of the molecules along the film. In order to avoid errors essentially due to the crossover with the soliton regime, we perform fits associated with a stability test. Provided that the film is thin enough ($N<5$), this method allows us to detect the difference between the widths of the splay domains according to their signs. With the tilt measurements, the widths of the splay domains of the two signs provide three independent determinations of the ratio K_1/b for each film thickness, so that gathering all our results, we finally get nine independent estimations for the linear splay elastic constant. We evaluate $K_1 \sim -(-1)^N \times 10^{-11}$ N, that moreover is of the same order of magnitude as the theoretical estimate based on the interactions between the molecules. As Fig. 10 shows, all these independent determinations are globally consistent with one another. They therefore give a supplementary proof of validity of our model.

Very interestingly, the sign alternation of K_1 with the parity of N, the number of smectic layers in the film, indicates that this linear splay elasticity is localized at the smectic-isotropic interface, and that the molecules of the smectic layer in contact with the isotropic subphase prefer to adopt a more converging configuration at larger tilts. This effect may be related to a reduced solubility of the aliphatic tips of the smectic molecules inside the isotropic phase at larger tilts, which could result from two mechanisms: a locally increased orientational order that consequently increases the difference from the isotropic phase, and a larger London interaction that draws the molecular tips closer to one another. So the K_1 effect appears to be extremely localized, inside the molecular tip layer, i.e., within ~ 1 nm, and therefore it may be mentioned as a 2D effect without exaggeration.

The value found for the linear elastic constant, K_1, is indeed very small. Nevertheless, it proves to have appreciable consequences in thin systems. Here, K_1 is shown to be able to promote a mechanical instability in the surface-induced films of MHTAC. As preliminary experiments show, such a result may be extended to other types of films provided that they have a polar symmetry. For instance, we observe similar spontaneous distortions in ferroelectric free-standing films of chiral smectic-C^* liquid crystals, but then the role of the director is played by the ferroelectric polarization, which is perpendicular to the molecular direction [40]. As a consequence, the linear elasticity now arises on the bend distortions instead of the splay ones, and the associated parameter may be called a *spontaneous bend elastic constant*. Also, the polarization being a volume property, the linear elasticity is no longer a surface effect in this case. However, two complications then arise, because of the superimposed helical distortion perpendicular to the film, and because of the electric space charges that arise in the places where the polarization adopts a divergent configuration, i.e., in the bend domains. Now being a volume effect, the space charges are no longer negligible. They strongly interact so that, above some threshold, an *electric instability* adds up to the previous elastic instability. The symmetry between the charges is broken, the charges of one sign no longer being located at equal distances from the charges of the other sign. The widths of both splay domains become consequently unequal as the widths of the bend domains were already, so that, on the whole, each splay or bend domains of the distortion have different widths.

An intermediate and interesting case to be mentioned is the case of the chiral SmC_A^* free-standing films with an odd number of layers, N. Being alternate, all the smectic layers compensate for each other but one, so that, on the whole, the film is asymmetric. In particular, it exhibits antiferroelectricity with a transverse polarization [29]. Such a film should therefore present a linear elasticity that differentiates the two bend distortions as in the SmC^* free-standing films discussed above, but now with a linear bend elastic constant that is independent of the film thickness instead of being proportional to N.

Such a physics is not restricted to liquid crystal films. Clearly, it may be observed in Langmuir films of tilted molecules, since they also exhibit polar symmetry. A reanalysis of the instabilities observed by Tabe and co-workers [8] on Langmuir films of 8AZ5, yields a ratio $|K_1/b| \sim 0.4$ μm (see Ref. [31]) in the same order of magnitude as the value measured here in the MHTAC surface-induced films, $|K_1/b(N=1)| \sim 1$ μm. One may also extend this result to particular biological films, provided that the molecules are locally oriented in the same tilted direction, and that they have a polar symmetry. However this last point should be easily fulfilled after the first one, since the biological films often separate different media, and are therefore essentially dissymmetric. Some examples of such a liquid crystalline behavior in biological membranes could be found during the numerous stages of formation of particular biological systems, or also in the mechanics of the electric impulse propagation along the nerve fibers [41]. This could structure the orientation of the molecules in asymmetric membranes without the help of chiral molecules.

ACKNOWLEDGMENT

We acknowledge helpful discussions with Dr. Y. Bouligand.

[1] M. Seul and D. Andelman, Science **267**, 425 (1995); M. Seul, L. R. Monar, L. O'Gorman, and R. Wolfe, *ibid.* **254**, 1616 (1991).

[2] See, for instance, P. G. de Gennes and J. Prost, *The Physics of Liquid Crystals* (Clarendon Press, Oxford, 1993).

[3] X. Qiu, J. Ruiz-Garcia, K. J. Stine, C. M. Knobler, and J. V. Selinger, Phys. Rev. Lett. **67**, 703 (1991).

[4] K.-K. Loh and J. Rudnick, Phys. Rev. Lett. **81**, 4935 (1998).

[5] I. Kraus and R. B. Meyer, Phys. Rev. Lett. **82**, 3815 (1999).

[6] C. Knobler, Physica A **236**, 11 (1997).

[7] O. D. Lavrentovich and V. M. Pergamenshchik, Phys. Rev. Lett. **73**, 979 (1994); Int. J. Mod. Phys. B **9**, 2389 (1995).

[8] Y. Tabe, N. Shen, E. Mazur, and H. Yokoyama, Phys. Rev. Lett. **82**, 759 (1999); Y. Tabe and H. Yokoyama, Mol. Cryst.

Liq. Cryst. **358**, 125 (2001).
[9] C. Y. Young, R. Pindak, N. A. Clark, and R. B. Meyer, Phys. Rev. Lett. **40**, 773 (1978).
[10] J. Maclennan and M. Seul, Phys. Rev. Lett. **69**, 2082 (1992); **69**, 3267 (1992); J. Maclennan, U. Sohling, N. A. Clark, and M. Seul, Phys. Rev. E **49**, 3207 (1994).
[11] S. A. Langer and J. P. Sethna, Phys. Rev. A **34**, 5035 (1986).
[12] J. Maclennan, Europhys. Lett. **13**, 435 (1990).
[13] E. Demikhov, Europhys. Lett. **25**, 259 (1994).
[14] E. Gorecka, M. Glogarova, H. Sverenyak, and L. Lejcek, Ferroelectrics **178**, 101 (1996).
[15] J. Pang and N. A. Clark, Phys. Rev. Lett. **73**, 2332 (1994).
[16] Y. Galerne and L. Liébert, Phys. Rev. Lett. **64**, 906 (1990).
[17] J. Penfold, Rep. Prog. Phys. **64**, 777 (2001); J.-G. Dash, Contemp. Phys. **30**, 89 (1989).
[18] A. Arbaoui, V. Candel, H. T. Nguyen, and Y. Galerne (unpublished).
[19] R. Meyer and P. Pershan, Solid State Commun. **13**, 989 (1973).
[20] H. Pleiner and H. R. Brand, Europhys. Lett. **9**, 243 (1989).
[21] J. V. Selinger and R. L. B. Selinger, Phys. Rev. E **51**, R860 (1995), and references therein.
[22] R. Najjar and Y. Galerne, Mol. Cryst. Liq. Cryst. **328**, 489 (1999).
[23] A. E. Jacobs, G. Goldner, and D. Mukamel, Phys. Rev. A **45**, 5783 (1992).
[24] R. B. Meyer, L. Liébert, L. Strzelecki, and P. Keller, J. Phys. (France) Lett. **36**, L69 (1975).
[25] G. Barbero, I. Dozov, J.-F. Palierne, and G. Durand, Phys. Rev. Lett. **56**, 2056 (1986).
[26] R. B. Meyer, Phys. Rev. Lett. **22**, 918 (1969).
[27] P. O. Andreeva, V. K. Dolganov, C. Gors, R. Fouret, and E. I. Kats, Phys. Rev. E **59**, 4143 (1999).
[28] Y. Galerne, Europhys. Lett. **18**, 511 (1992).
[29] Y. Galerne and L. Liébert, Phys. Rev. Lett. **66**, 2891 (1991).
[30] Y. Galerne, I. Poinsot, and D. Schaegis, Appl. Phys. Lett. **71**, 222 (1997).
[31] R. Najjar and Y. Galerne, Europhys. Lett. **55**, 355 (2001); Mol. Cryst. Liq. Cryst. **367**, 395 (2001).
[32] V. Candel and Y. Galerne, Liq. Cryst. **15**, 541 (1993).
[33] A.-M. Levelut, C. Germain, P. Keller, L. Liébert, and J. Billard, J. Phys. (Paris) **44**, 623 (1983).
[34] A. Blumstein and L. Patel, Mol. Cryst. Liq. Cryst. **48**, 151 (1978).
[35] V. Candel and Y. Galerne, Phys. Rev. Lett. **70**, 4083 (1993).
[36] Y. Galerne (unpublished).
[37] Y. Galerne, Phys. Rev. A **24**, R2284 (1981).
[38] Y. Galerne, J. Phys. (France) Lett. **44**, L461 (1983).
[39] J.-F. Li, Ch. Rosenblatt, Z. Li, and Y. Suzuki, Phys. Rev. E **51**, 462 (1995).
[40] R. Najjar and Y. Galerne, Mol. Cryst. Liq. Cryst. **366**, 421 (2001).
[41] D. Ottoson, *Physiology of the Nervous System* (MacMillan Press, New York, 1983).